(704) Interamnia: a transitional object between a dwarf planet and a typical irregular-shaped minor body

J. Hanuš, P. Vernazza, M. Viikinkoski, M. Ferrais, N. Rambaux, E. Podlewska-Gaca, A. Drouard, L. Jorda, E. Jehin, B. Carry, et al.

A&A 633, A65 (2020)
https://doi.org/10.1051/0004-6361/201936639

Astronomy & Astrophysics

(704) Interamnia: a transitional object between a dwarf planet and a typical irregular-shaped minor body⋆,⋆⋆

J. Hanuš[1], P. Vernazza[2], M. Viikinkoski[3], M. Ferrais[4,2], N. Rambaux[5], E. Podlewska-Gaca[6], A. Drouard[2], L. Jorda[2], E. Jehin[4], B. Carry[7], M. Marsset[8], F. Marchis[9], B. Warner[10], R. Behrend[11], V. Asenjo[12], N. Berger[13], M. Bronikowska[14], T. Brothers[8], S. Charbonnel[15], C. Colazo[16], J.-F. Coliac[17], R. Duffard[18], A. Jones[19], A. Leroy[20], A. Marciniak[6], R. Melia[16], D. Molina[21], J. Nadolny[22], M. Person[8], O. Pejcha[23], H. Riemis[24], B. Shappee[25], K. Sobkowiak[6], F. Soldán[26], D. Suys[24], R. Szakats[27], J. Vantomme[24], M. Birlan[5], J. Berthier[5], P. Bartczak[6], C. Dumas[28], G. Dudziński[6], J. Ďurech[1], J. Castillo-Rogez[29], F. Cipriani[30], R. Fetick[2], T. Fusco[2], J. Grice[7,31], M. Kaasalainen[3], A. Kryszczynska[6], P. Lamy[32], T. Michalowski[6], P. Michel[7], T. Santana-Ros[33,34], P. Tanga[7], F. Vachier[5], A. Vigan[2], O. Witasse[30], and B. Yang[35]

(Affiliations can be found after the references)

Received 5 September 2019 / Accepted 21 November 2019

ABSTRACT

Context. With an estimated diameter in the 320–350 km range, (704) Interamnia is the fifth largest main belt asteroid and one of the few bodies that fills the gap in size between the four largest bodies with $D > 400$ km (Ceres, Vesta, Pallas and Hygiea) and the numerous smaller bodies with diameter ≤200 km. However, despite its large size, little is known about the shape and spin state of Interamnia and, therefore, about its bulk composition and past collisional evolution.

Aims. We aimed to test at what size and mass the shape of a small body departs from a nearly ellipsoidal equilibrium shape (as observed in the case of the four largest asteroids) to an irregular shape as routinely observed in the case of smaller ($D \leq 200$ km) bodies.

Methods. We observed Interamnia as part of our ESO VLT/SPHERE large program (ID: 199.C-0074) at thirteen different epochs. In addition, several new optical lightcurves were recorded. These data, along with stellar occultation data from the literature, were fed to the All-Data Asteroid Modeling algorithm to reconstruct the 3D-shape model of Interamnia and to determine its spin state.

Results. Interamnia's volume-equivalent diameter of 332 ± 6 km implies a bulk density of $\rho = 1.98 \pm 0.68$ g cm^{-3}, which suggests that Interamnia – like Ceres and Hygiea – contains a high fraction of water ice, consistent with the paucity of apparent craters. Our observations reveal a shape that can be well approximated by an ellipsoid, and that is compatible with a fluid hydrostatic equilibrium at the 2σ level.

Conclusions. The rather regular shape of Interamnia implies that the size and mass limit, under which the shapes of minor bodies with a high amount of water ice in the subsurface become irregular, has to be searched among smaller ($D \leq 300$ km) less massive ($m \leq 3 \times 10^{19}$ kg) bodies.

Key words. minor planets, asteroids: individual: (704) Interamnia – methods: observational – techniques: high angular resolution – techniques: photometric

1. Introduction

Because of their large masses, Solar-System bodies with diameters larger than ∼900 km possess rounded, ellipsoidal shapes, consistent with hydrostatic equilibrium. On the other side of the mass range, very small bodies (diameters ≤100 km) tend to possess highly irregular shapes, with the notable exception of some $D \leq 5$ km bodies that are affected by the so-called YORP effect (Yarkovsky–O'Keefe–Radzievskii–Paddack, Rubincam 2000; Vokrouhlický et al. 2003), and which have similar shapes to a spinning top (e.g., Ryugu, or Bennu, Watanabe et al. 2019; Nolan et al. 2013). The theory of the hydrostatic equilibrium of homogeneous bodies is well established (e.g., Chandrasekhar 1969), whereas for differentiated bodies, approaches based on Clairaut equations (e.g., Dermott 1979; Chambat et al. 2010; Rambaux et al. 2015, 2017) or the numerical non-perturbative method are still under developement (Hubbard 2013). From an observational point of view, it remains to be tested at what size range the shape of a typical minor body transits from a nearly rounded equilibrium shape to an irregular shape and to what extent this size range depends on factors such as the bulk composition of the minor planet or its collisional and thermal history.

Investigating these questions is one of the main motivations of our European Southern Observatory (ESO) large program (id: 199.C-0074; Vernazza et al. 2018) of which the aim is to constrain the shape of the forty largest main-belt asteroids. So far, our program has revealed that (10) Hygiea, the fourth largest main-belt asteroid (D ∼ 434 km) possesses a shape that is nearly as spherical as that of (1) Ceres (Vernazza et al. 2019), while being twice as small, whereas $D \sim$ 100–200 km bodies

⋆ The reduced images are only available at the CDS via anonymous ftp to cdsarc.u-strasbg.fr (130.79.128.5) or via http://cdsarc.u-strasbg.fr/viz-bin/cat/J/A+A/633/A65

⋆⋆ Based on observations made with ESO Telescopes at the La Silla Paranal Observatory under program 199.C-0074 (PI: Vernazza).

[(89) Julia, (16) Psyche, (41) Daphne] possess irregular shapes (Vernazza et al. 2018; Viikinkoski et al. 2018; Carry et al. 2019). Asteroid (7) Iris ($D \sim 214$ km) is an intermediate case, as its shape appears to be consistent with that of an oblate spheroid with a large equatorial excavation (Hanuš et al. 2019).

Asteroid (704) Interamnia, the fifth largest body in the main belt with a volume equivalent diameter in the 320–350 km size range (Drummond et al. 2009; Masiero et al. 2014), is one of the very few asteroids that fills the gap in size between Hygiea and $D \sim 250$ km-sized bodies. The remaining main belt asteroids in this size range are (31) Euphrosyne ($D = 282 \pm 10$ km, Masiero et al. 2013), (52) Europa ($D = 314 \pm 5$ km, Hanuš et al. 2017), (65) Cybele ($D = 296 \pm 25$ km, Viikinkoski et al. 2017), and (511) Davida ($D = 311 \pm 5$ km, Viikinkoski et al. 2017). Shapes of Europa and Davida already show some departures from a rotational triaxial ellipsoid (Conrad et al. 2007; Merline et al. 2013). Interamnia thus appears as another key target for investigating at what size the shape of a small body becomes irregular.

So far, little is known about Interamnia. It lacks a dynamical family, implying that it avoided a giant impact over the last ~3 Gyrs. It was classified in the B-spectral class following the Bus taxonomy based on visible data alone, whereas it is labeled a C-type in the Bus-DeMeo taxonomy (Clark et al. 2010). In the visible and near-infrared spectral range, it thus appears similar to objects such as (1) Ceres, (10) Hygiea, (24) Themis, and (52) Europa, which have been connected to interplanetary dust particles (IDPs) rather than to carbonaceous chondrites (Vernazza et al. 2015, 2017; Marsset et al. 2016). Interamnia is also of great interest to the present study, being the largest asteroid for which a detailed shape model (convex or with local topography) and consistent spin-state solutions do not yet exist. This may be due to its shape being rather spherical, as suggested by the small brightness variations in its lightcurves (Tempesti 1975; Warner 2018) and by the Keck disk-resolved images obtained by Drummond & Christou (2008).

Here, we present high-angular resolution imaging observations of Interamnia with ESO VLT/SPHERE/ZIMPOL that were performed as part of our large program. We use these observations along with several newly acquired lightcurves to constrain its 3D shape and its spin for the first time.

2. Observations

The observations used in our analysis of physical properties of Interamnia consist of disk-resolved images from the VLT telescope and disk-integrated optical lightcurves from various sources, including our observing campaign.

2.1. Disk-resolved data

Interamnia was observed with VLT/SPHERE/ZIMPOL (Spectro-Polarimetric High-contrast Exoplanet REsearch, Zurich IMaging POLarimeter, Thalmann et al. 2008) in the narrow band imaging configuration (N_R filter; filter central wavelength = 645.9 nm, width = 56.7 nm) during two consecutive apparitions in August–September 2017, and between December 2018 and January 2019. During both apparitions, the angular size of Interamnia was in the 0.20–0.26″ range, with a slightly larger angular size during the first apparition. Interamnia's extent on the images reaches up to 80 pixels. Both datasets sample the whole rotation phase of Interamnia, although not as evenly as initially expected (we recall here that our nominal observing strategy is to image our large program targets every 60 degrees throughout their rotation). Nonetheless, the satisfactory rotation phase coverage, along with a nearly equator-on geometry during both apparitions lead to a nearly complete surface coverage (~95%) that makes it possible to constrain the three dimensions of Interamnia well.

The reduced images were deconvolved with the `Mistral` algorithm (see Fétick et al. 2019, for details about the deconvolution procedure) and are shown in Figs. A.1 and A.2. Table A.1 contains full information about the data.

Finally, in addition to the AO data, we also utilized four stellar occultations obtained in 1996, 2003, 2007, and 2012. However, the stellar occultations are largely redundant given the coverage of our SPHERE observations. We provide details about these observations in Table A.2.

2.2. Optical photometry

We compiled a large dataset of 189 optical lightcurves sampling 15 apparitions. These data include lightcurves downloaded from the Asteroid Photometric Catalog (APC, Piironen et al. 2001) with original references: Tempesti (1975); Lustig & Hahn (1976); Shevchenko et al. (1992); Michalowski et al. (1995). Many lightcurves were also provided through the courbes de rotation d'astéroïdes et de comètes database (CdR[1]), maintained by Raoul Behrend at the Observatoire de Genève, and through the ALCDEF[2] database maintained by Brian Warner (Warner 2018). The largest photometric dataset was obtained from the SuperWASP archive (Grice et al. 2017): 114 lightcurves spanning years 2006–2011. Finally, one lightcurve was obtained at Wallace Observatory, and a densely covered dataset was obtained by the TRAPPIST-South and -North (Jehin et al. 2011) as a support for this study.

Additional photometric data were gathered within the observing campaign of the "Small Bodies: Near And Far" project (Müller et al. 2018), with partial participation of *Gaia*-GOSA observers. *Gaia*-GOSA[3] is a web service dedicated to amateur observers willing to support asteroid studies through targeted photometric campaigns. The website makes it possible to coordinate a worldwide observing campaign, which is especially important for slow rotating objects requiring long-term observations over several nights. Interamnia was observed on *Gaia*-GOSA during its last two apparitions (2017 and 2018), providing new lightcurves for our dataset.

Finally, we also made use of sparsely sampled V-band photometry from the All-Sky Automated Survey for Supernovae (ASAS-SN, Shappee et al. 2014; Kochanek et al. 2017) and *Gaia* Data Release 2 (DR2, Gaia Collaboration 2018). The ASAS-SN data sample five consequent apparitions between 2013 and 2018, and contain 196 individually calibrated measurements in the Johnson V band. *Gaia* DR2 data are internally calibrated, however, they are also limited to only 16 individual measurements. The sparse data are processed following the same procedures applied, for example, in Hanuš et al. (2011), or Ďurech & Hanuš (2018). Other sparsely sampled data used so far for the shape modeling (e.g., USNO-Flagstaff, Catalina Sky Survey, Lowell, Ďurech et al. 2009, 2016; Hanuš et al. 2011, 2013) have photometric uncertainties, at best, comparable to the lightcurve amplitude of Interamnia (usually <0.1 mag), which makes them useless for the shape modeling. On the other hand, the high-photometric precision of the ASAS-SN data (~0.04 mag) and *Gaia* DR2 (~0.02 mag) implies that brightness changes due to irregular

[1] http://obswww.unige.ch/~behrend/page_cou.html
[2] http://alcdef.org/
[3] www.gaiagosa.eu

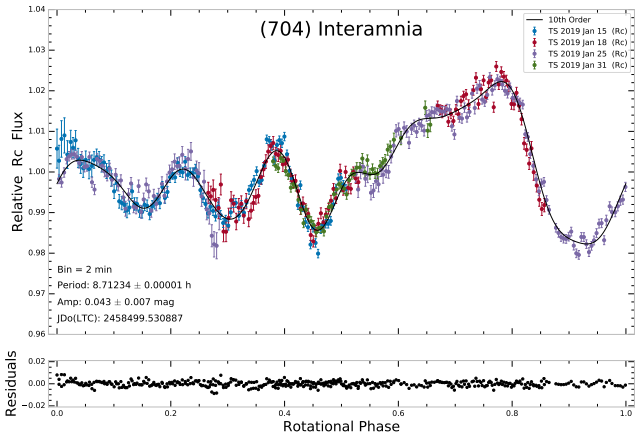

Fig. 1. *Upper panel*: composite lightcurve of (704) Interamnia obtained with TRAPPIST-South telescope. A Fourier series of tenth order is fitted to the data. *Lower panel*: residuals of the fit.

shape and spin state are distinguishable from the photometric noise. Sparse data are particularly useful for the spin-state determination, because they cover a large range of observing geometries (i.e., phase angles).

The basic characteristics of the photometric data are listed in Table A.3. In general, Interamnia's lightcurves exhibit a brightness variation pattern consistent with a synodic rotation period of ~8.7 h and rather small amplitude of the brightness changes within the rotation (usually <0.1 mag, see, e.g., Fig. 1). These small changes make the determination of a unique shape model and spin-state solution challenging.

3. Results

The rich datasets of disk-integrated optical lightcurves and VLT/SPHERE/ZIMPOL disk-resolved images enabled us to derive the convex shape model of Interamnia, as well as its 3D-shape model with local topography. Moreover, we also estimated Interamnia's bulk density and analysed its shape with respect to the hydrostatic equilibrium. Finally, we discuss few identified surface features.

3.1. Spin-state determination by convex inversion

To derive the first reliable shape and spin-state solution for Interamnia, we implemented the standard convex inversion method of Kaasalainen & Torppa (2001) and Kaasalainen et al. (2001) that takes disk-integrated data as the only data input, and searches the set of parameters describing the shape and rotation state that best match the data. The search was done on a grid of parameters, where each set of input parameters converges to a local minimum in the parameter space. We tested all reasonable combinations of relevant parameters to find those that correspond to the global minimum. In convex inversion, the shape is parametrized by a convex polyhedron, the rotation state is described by the sidereal rotation period, and the ecliptic coordinates (longitude and latitude) of the spin axis, and we used a simple three-parameter phase function relation that is necessary when sparse data are included (Kaasalainen et al. 2001). The convex inversion procedure essentially consists of two parts. Firstly, we ran the convex inversion for rotation periods from the 8.6–8.8 h interval, which contains all previous estimates that concentrate near ~8.72 h. The step in the rotation period was selected in a way that each local minimum is sampled (Kaasalainen et al. 2001). For each period, we ran the convex inversion with 10 different initial pole orientations isotropically distributed on a sphere and selected only the best fitting solution. Then, we constructed the dependence of the rms value on the sampled period in Fig. A.3. This periodogram has a clear minimum near 8.71 h, moreover, only one period value (P = 8.71236 h) provides a significantly better fit to the observed data than all the other periods. We applied the same criteria as in Hanuš et al. (2018, for more details and additional references) to distinguish between acceptable solutions and those that should already be rejected. Secondly, we ran the convex inversion with the unique period found in the previous step, with a higher shape model resolution, and for many pole orientations (~50) isotropically distributed on a sphere. Only four pole solutions fell within the rms limit from Hanuš et al. (2018). Moreover, two solutions out of the four with the worst fit had non-physical shapes with their maximum moment of inertia significantly nonaligned with the rotation axis. Therefore, we derived only two possible spin-state and shape solutions, which we list in Table 1.

Our spin-state solutions are rather different from those previously published with the main disagreement in the ecliptic latitude – we found a prograde rotation with ecliptic latitude of ~40–60°, while previous authors derived mostly smaller values between –20° and 20° (Michalowski 1993; Michalowski et al. 1995; De Angelis 1995; Drummond & Christou 2008), or even –50° (Satō et al. 2014) for the latitude. On the other hand, the determinations for the ecliptic longitude are mostly consistent with each other. The closest solution to ours is from Drummond et al. (2009) based on disk-resolved images from Keck. The rather significant differences are likely caused by (i) Interamnia having small brightness variations, and (ii) the fact that the spin-state determination based on photometric data with low signal-to-noise ratio is challenging and could lead to inaccurate determinations (or to underestimated uncertainties, Marciniak et al. 2015). Our first reliable spin-state solution of Interamnia is used as an input for the shape modeling with All-Data Asteroid Modeling (ADAM) in the following section.

3.2. 3D-shape reconstruction with ADAM

The disk-resolved data allow us to perform the 3D-shape optimization with the ADAM algorithm. Firstly, we compared the SPHERE images with corresponding projections of the two shape solutions derived by the convex inversion and found that only one solution is consistent with the images (see Table. 1), therefore, we continued the shape modeling only with the preferred rotation state solution as an input.

We proceeded with the modeling the standard way (see, e.g., Viikinkoski et al. 2018; Hanuš et al. 2019): we constructed a low-resolution shape model using the octantoid (Viikinkoski et al. 2015a) shape parametrization while balancing the fit to the optical lightcurves, SPHERE images, and stellar occultations. We applied the ADAM algorithm to a dataset of 189 optical lightcurves, 60 VLT/SPHERE/ZIMPOL images, and four stellar occultations. Then, we increased the shape model resolution and the weight of the SPHERE data with respect to the lightcurves and occultations, and used the low-resolution shape model as an initial input. We tested several combinations of shape resolutions and relative weighting of the observed data to confirm the consistency of our results. The comparison between the shape model projections and SPHERE observations is shown in Fig. 2. Moreover, we also provide the model fit to the stellar occultations in Fig. 3. All four stellar occultations agree well with our shape model.

Table 1. Summary of published spin-state solutions for Interamnia.

λ_1 (deg)	β_1 (deg)	λ_2 (deg)	β_2 (deg)	P (h)	Note
43 ± 8	-21 ± 9	224 ± 10	-22 ± 10	–	Michalowski (1993)
47 ± 10	-3 ± 10	227 ± 10	1 ± 10	–	De Angelis (1995)
51 ± 15	22 ± 10			8.72729 ± 0.00001	Michalowski et al. (1995)
36 ± 5	12 ± 5			–	Drummond & Christou (2008)
47 ± 10	66 ± 10			–	Drummond et al. (2009)
259 ± 8	-50 ± 5			$8.728967167 \pm 0.000000007$ [(a)]	Satō et al. (2014)
87 ± 10	63 ± 10	~~226 ± 10~~	~~43 ± 10~~	8.712355 ± 0.000005	This work, CI
87 ± 5	62 ± 5			8.71234 ± 0.00001	This work, ADAM

Notes. The table gives the ecliptic longitude λ and latitude β of all possible pole solutions with their uncertainties, the sidereal rotation period P, and the reference. Our second pole solution from convex inversion (CI) has been rejected due to inconsistency with the SPHERE images. [(a)]Such uncertainty in the rotation period is unrealistic.

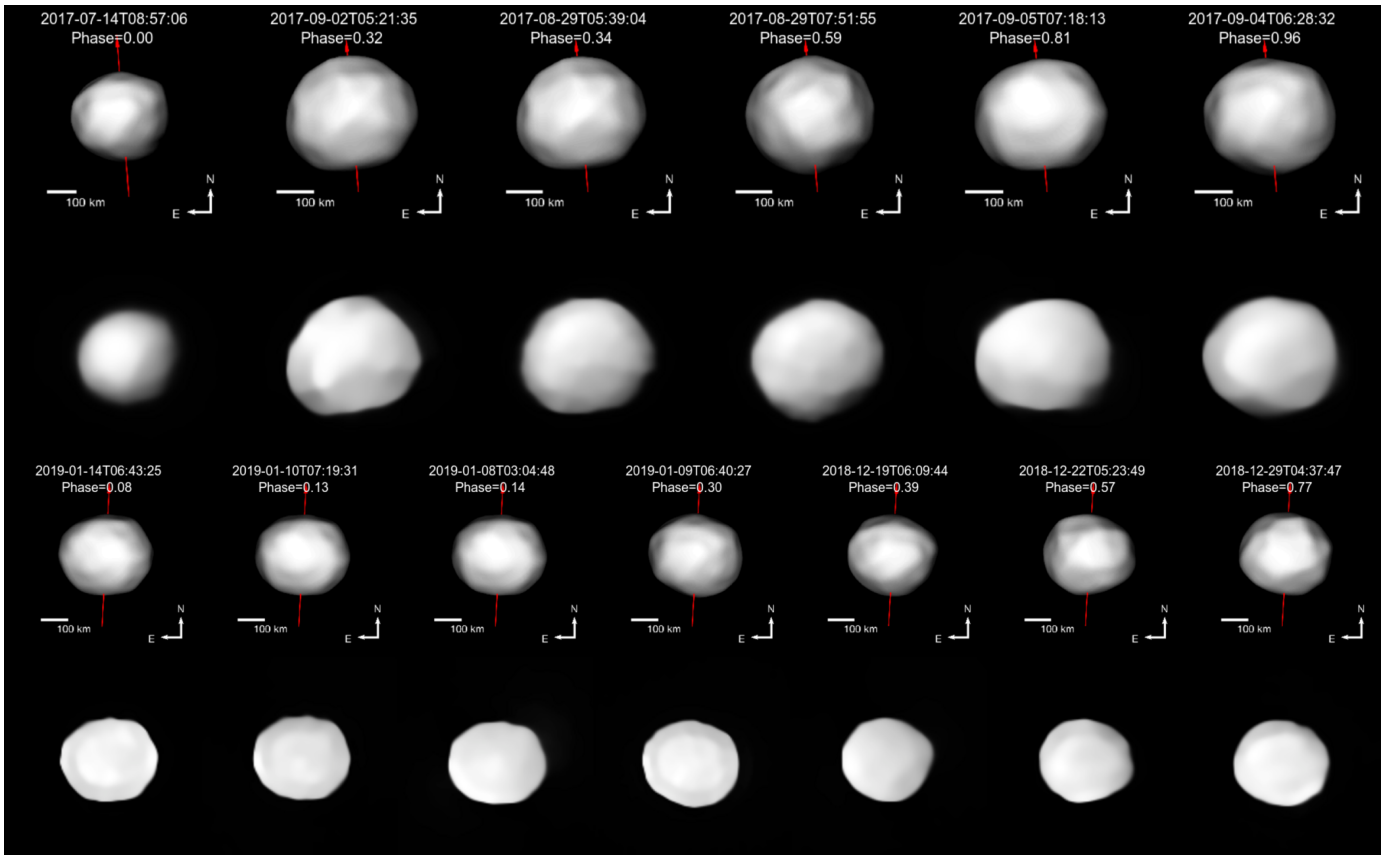

Fig. 2. Comparison between VLT/SPHERE/ZIMPOL deconvolved images of Interamnia (*second and fourth rows*) and the corresponding projections of our ADAM shape model (*first and third row*). The red line indicates the position of the rotation axis. We use a nonrealistic illumination to highlight the local topography of the model.

The physical properties of our final solution are listed in Table 2. The uncertainties reflect the typical ranges of parameters within the various individual solutions we obtained (for different shape resolutions, relative data weights). The uncertainties are also consistent with the size of one to two pixels. The volume-equivalent diameter of Interamnia (332 ± 6 km) is well constrained because of the equator-on observations during both apparitions, and because the overall coverage of the AO observations amounts to ~95% of the model surface area. Moreover, for the same reason, the c dimension is also reliably estimated, which happens rather rarely, because the usually limited geometry coverage of the images makes the determination of the c dimension inaccurate. Our size estimate is larger than those of Drummond et al. (2009) and Satō et al. (2014), but both are in agreement with ours within the 1σ uncertainties.

The shape model along with the lightcurve data and the fit to all datasets have been uploaded to the online Database of Asteroid Models from Inversion Techniques (DAMIT[4], Ďurech et al. 2010).

[4] http://astro.troja.mff.cuni.cz/projects/damit

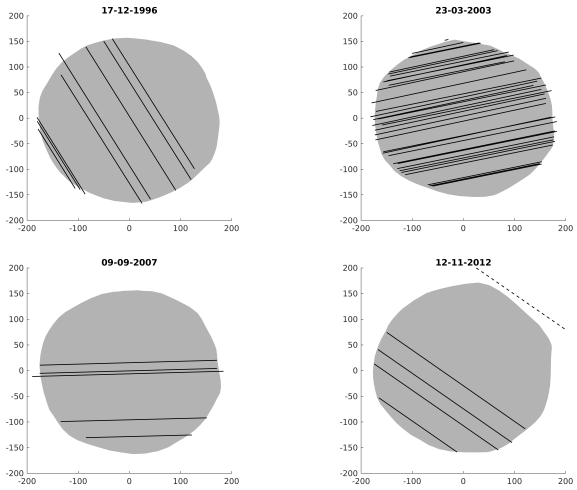

Fig. 3. Observed occultation chords and model silhouettes. The dashed line is a negative observation. North is up and east to the left. The axis scale corresponds to kilometers.

3.3. Density

We combined the derived volume of Interamnia with the best estimate of its mass $(3.79 \pm 1.28) \times 10^{19}$ kg (Table A.4 and Fig. A.4) and obtained a bulk density estimate of 1.98 ± 0.68 g cm^{-3}. Our mass estimate is based on all relevant determinations collected in the literature (as we did in our previous studies, for instance, Carry et al. 2012; Vernazza et al. 2018; Viikinkoski et al. 2018; Hanuš et al. 2019).

The relative uncertainty affecting the bulk density of Interamnia exceeds 30%, preventing us from drawing meaningful conclusions about the body's composition. For instance, the bulk density is compatible within 1σ error with those of the two largest C-type asteroids, Ceres (2.161 ± 0.003 g cm^{-3}, Park et al. 2019) and Hygiea (1.94 ± 0.25 g cm^{-3}, Vernazza et al. 2019), but also of silicate bodies such as (25143) Itokawa (1.90 ± 0.13 g cm^{-3}, Fujiwara et al. 2006) or (433) Eros (2.67 ± 0.10 g cm^{-3}, Veverka et al. 2000). Current estimates of the densities of asteroids with masses greater than $\sim 5 \times 10^{18}$ kg imply a small amount of macroporosity within these bodies (Carry 2012; Viikinkoski et al. 2015b; Marsset et al. 2017; Carry et al. 2019; Hanuš et al. 2019), and spectroscopic observations of Interamnia in the 3-micron region have revealed the presence of hydrated material at its surface (Usui et al. 2019) and spectral similarity to Ceres (Rivkin et al. 2019). Therefore, we can assume that Interamnia's bulk density is close to that of Ceres. This implies a large amount of water inside Interamnia, likely as a mixture of ice and phyllosilicates, as in the case of Ceres.

3.4. Shape analysis

As a first step, we performed an analysis of Interamnia's shape, similar to the one performed in the case of Hygiea (Vernazza et al. 2019). We fitted Interamnia's 3D-shape model with an ellipsoid and subsequently measured the radial difference between the two shapes. It appears that the large-scale topography of Interamnia is very subdued, without noticeable large impact basins on its surface (Fig. A.5), similar to that of Ceres and Hygiea (Vernazza et al. 2019). As in the case of Hygiea, the relative volume difference between Interamnia's 3D-shape model and that of its best-fitting ellipsoid is 0.2%, which implies that Interamnia's shape is very close to that of an ellipsoid. Next, we calculated the sphericity of Interamnia as done previously in the case of Hygiea (Vernazza et al. 2019). We found a sphericity value of 0.9880, similar to that of Vesta (0.9860), and only marginally lower than that of the nearly spherical dwarf planet candidate Hygiea (0.9975, Vernazza et al. 2019).

Given the ellipsoidal shape of Interamnia and the fact that its a and b axes have similar lengths (within errors) and that the c dimension is shorter than the a and b axes, we investigated whether Interamnia's shape may be at hydrostatic equilibrium. We investigated both (i) a homogeneous and (ii) a core-mantle differentiated case. Indeed, given the large uncertainty of the bulk density coming from the large mass uncertainty, both models are viable possibilities.

The hydrostatic equilibrium figure of an homogeneous body can be computed using MacLaurin's equation (e.g., Chandrasekhar 1969):

$$\frac{\Omega^2}{\pi G \rho} = \frac{2\sqrt{1-e^2}}{e^3}(3-2e^2)\arcsin(e) - 6\frac{1-e^2}{e^2}, \quad (1)$$

where G is the gravitational constant, Ω is the rotational velocity, and e is the ellipticity of the body shape defined by

$$e^2 = 1 - \left(\frac{c}{a}\right)^2. \quad (2)$$

The MacLaurin equation is not valid for a differentiated body (Moritz 1990). In this case, the hydrostatic equilibrium figure can be derived through Clairaut's equations developed to an order that depends on a parameter m called geodetic parameter (Chambat et al. 2010; Rambaux et al. 2015):

$$m = \frac{\Omega^2 R^3}{GM}, \quad (3)$$

where Ω is the angular spin velocity, R the mean radius, and M the mass of the body. Considering the particular value of m and the quality of available observations, Clairaut's equations may be developed to first, second, or third order (Lanzano 1974). For example, at first order, Clairaut's equation is written as (Kopal 1960; Lanzano 1974)

$$r^2 \ddot{f}_2 + 6\gamma r \dot{f}_2 + 6(\gamma - 1) f_2 = 0, \quad (4)$$

where f_2 corresponds to the coefficient of the Legendre polynomial of degree two of the equipotential surface s

$$s(r, \theta) = r(1 + f_2(r) P_2(\cos\theta)), \quad (5)$$

and $\gamma = \rho(r)/\bar{\rho}(r)$ is the ratio between the density of the layer at r and the mean density at r. Lanzano (1974) developed the equations up to order three by introducing the following coefficients:

$$s(r, \theta) = r(1 + f_2(r) P_2(\cos\theta) + f_4(r) P_4(\cos\theta) + f_6(r) P_6(\cos\theta)), \quad (6)$$

and he obtained a system of three differential equations and boundary conditions (see the equations in Lanzano 1974). A numerical scheme to solve these equations has previously been applied to the hydrostatic figures of Earth (Chambat et al. 2010), Ceres (Rambaux et al. 2015; Park et al. 2016) and Pallas (Marsset et al., in prep.), and now to a differentiated Interamnia.

For the homogeneous case, we computed a–c values for mean densities within the 1300–2700 kg m^{-3} range, while for the core-mantle differentiated model, we explored the 1100–1600 kg m^{-3} range for the mantle density and the

Table 2. Volume-equivalent diameter (D), dimensions along the major axis (a, b, c), sidereal rotation period (P), spin-axis ecliptic J2000 coordinates (longitude λ and latitude β), mass (m), and bulk density (ρ) of Interamnia as determined here, compared with the work of Drummond & Christou (2008); Drummond et al. (2009); Satō et al. (2014).

Parameter	Unit	Drummond & Christou (2008)	Drummond et al. (2009)	Satō et al. (2014)	This work, ADAM
D	km		319 ± 9	327 ± 3	332 ± 6
λ	deg.	36 ± 6	47 ± 3	259 ± 8	87 ± 5
β	deg.	12 ± 11	66 ± 3	-50 ± 5	62 ± 5
P	h		8.727	8.728967167(7)	8.712336(10)
a	km	385 ± 53	349 ± 4	362 ± 3	362 ± 8
b	km	337 ± 21	339 ± 3	324 ± 5	348 ± 8
c	km	163 ± 184	274 ± 22	297 ± 4	310 ± 8
a/b		1.14 ± 0.17	1.03 ± 0.01	1.15 ± 0.02	1.04 ± 0.02
b/c		2.1 ± 2.3	1.24 ± 0.10	1.20 ± 0.01	1.13 ± 0.02
m	10^{19} kg			6.96 ± 1.79 [(a)]	3.79 ± 1.28
ρ	g cm^{-3}			3.8 ± 1.0	1.98 ± 0.68

Notes. Uncertainties correspond to 1σ values.
References. [(a)]Michalak (2001).

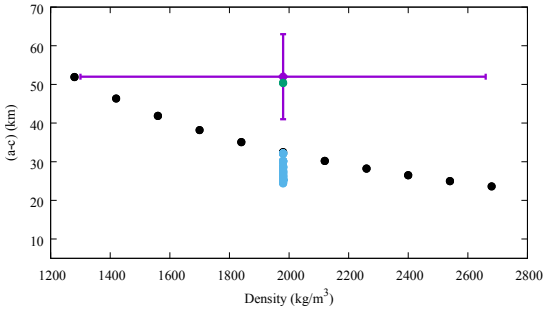

Fig. 4. Results of $(a-c)$ for Interamnia as a function of mean density for homogeneous case (sequence of black dots) and core-mantle differentiated case (blue vertical dots). For the latter case, we explored the 1100–1600 kg m^{-3} range for the mantle density, and the 2050–3400 kg m^{-3} range for the core density while keeping the bulk density at a constant value of 1980 kg m^{-3}. The value of $a-c$ decreases when mass increases with depth. The purple cross represents the value derived in Sect. 3.4 with its 1σ uncertainty (uncertainties of a and b are added quadratically). Finally, the green dot represents the values of $(a-c)$ for the homogeneous case and Interamnia's assumed faster rotation period of 7.1 h.

2050–3400 kg m^{-3} range for the core density while keeping the bulk density at 1 980 kg m^{-3}. As expected, $a-c$ decreases when mass increases with depth. In Fig. 4, we present the $a-c$ values as a function of mean density for both the homogeneous case (black dots) and the core-mantle differentiated case (blue dots) and compare them with the observed values.

Assuming Interamnia's bulk density of 2000 kg m^{-3} (i.e., similar to that of Ceres or Hygiea), its shape is consistent with hydrostatic equilibrium at the 2σ level. We further calculated, by aiming for the central value of $a-c$, that Interamnia's shape would be at hydrostatic equilibrium at the 1σ level for a slightly shorter rotation period (7.1 h, see Fig. 4), assuming homogeneous interior. The core-mantle differentiated case requires slightly larger despinning. This is in agreement with the collisional models that predict statistical preference of despinning by impacts (Ševeček et al. 2019).

Overall, these results are compatible with a formation of Interamnia at hydrostatic equilibrium. Interamnia's global equilibrium shape is likely a consequence of both its large mass and the initial presence of a large amount of water ice in its interior. During its early history, a large fraction of the water ice would have melted due to the radioactive decay of ^{26}Al implying the presence of liquid water in its interior, and thus an early fluid interior as is the case for Vesta, Ceres, and Hygiea (Takir & Emery 2012; Vernazza et al. 2017).

3.5. Surface topography

We observe only two large depressions (apparent dark regions) in the bottom-right parts of the images with rotation phases 0.32 and 0.96 (first apparition). In addition, a few mountain-like features can be observed in the object's contours. The most prominent one lies very close to the north pole and is visible at three epochs from the second apparition (rotation phases 0.08, 0.13 and 0.14). This feature could be a central peak of a ~150–200 km large crater. Two similar topographic features are located to the bottom right of the image at rotation phase 0.77 (second apparition), and on the right of rotation phase 0.57 (Fig. 5).

Compared with the large topographic variations found on S-type asteroids such as (3) Juno, (6) Hebe, and (7) Iris (Viikinkoski et al. 2015b; Marsset et al. 2017; Hanuš et al. 2019), Interamnia's surface appears relatively smooth with only a few basins or depressions. From this point of view, Interamnia appears very similar to Hygiea and Ceres (Vernazza et al. 2019). A plausible explanation for the lack of obvious craters at the resolution of these SPHERE images may be, as proposed in the case of Hygiea (Vernazza et al. 2019), that the craters are mostly complex flat-floored rather than simple bowl-shaped. The expected simple-to-complex crater transition diameter for Interamnia, assuming a water-rich composition for its mantle in agreement with our density estimate, should be around 30 km (Hiesinger et al. 2016) (the transition diameter for a rock-dominated composition would be around 70 km). Given the spatial resolution of our observations ($D \sim 30$–40 km), the paucity of large bowl-shaped craters on Interamnia can be attributed to its water-rich mantle composition.

4. Summary

We derived the first reliable spin-state solution of Interamnia. This success was only possible due to a large participation in

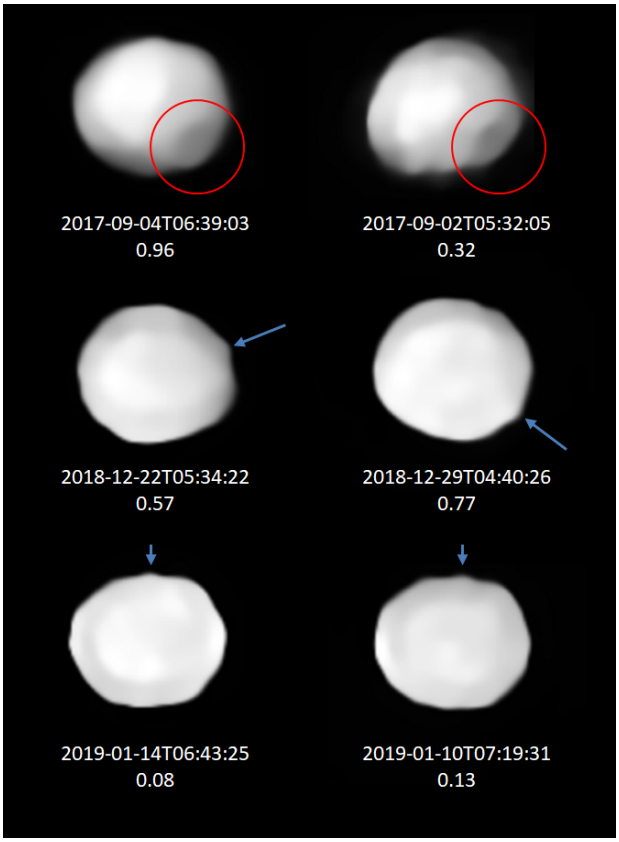

Fig. 5. Topographic features identified on Interamnia. The arrows indicate potential surface features (central peaks of large impact basins) and the red circles the two darker circular regions.

our photometric campaign and data mining from survey telescopes (SuperWASP, ASAS-SN, *Gaia*). The role of observers with small aperture telescopes was essential.

Our 3D-shape model of Interamnia derived by ADAM from the spectacular SPHERE disk-resolved images is nearly ellipsoidal with almost equal equatorial dimensions ($a/b = 1.04$) and is only slightly flattened with $b/c = 1.13$. Interamnia's shape appears to be in hydrostatic equilibrium at the 2σ level. It follows that the size and mass limit under which minor bodies' shapes become irregular has to be searched among smaller ($D \leq 300$ km) less massive ($m \leq 3 \times 10^{19}$ kg) bodies.

Our volume equivalent diameter of 332 ± 6 km makes Interamnia the fifth largest object in the main belt after (1) Ceres, (2) Pallas, (4) Vesta, and (10) Hygiea. The other two 300-km-class bodies – (52) Europa and (65) Cybele – are likely smaller than Interamnia, although their size estimates have rather large uncertainties. Finally, spectroscopic observations in the near infrared and the bulk density of $\rho = 1.98 \pm 0.68$ g cm^{-3} suggests that Interamnia – like Ceres and Hygiea – contains a high fraction of water in the subsurface. This would provide a natural explanation for the lack of obvious craters wider than a few tens of km, as well as for its ellipsoidal/regular shape, similarly to what has been proposed for Hygiea by Vernazza et al. (2019).

Acknowledgements. This work has been supported by the Czech Science Foundation through grant 18-09470S (J.H., J.D.) and by the Charles University Research program No. UNCE/SCI/023. This research was supported by INTER-EXCELLENCE grant LTAUSA18093 from the Czech Ministry of Education, Youth, and Sports (J.H. and O.P.). The research of O.P. is additionally supported by Horizon 2020 ERC Starting Grant "Cat-In-hAT" (grant agreement #803158) and award PRIMUS/SCI/17 from Charles University. P.V., A.D., and B.C. were supported by CNRS/INSU/PNP. M.M. was supported by the National Aeronautics and Space Administration under Grant No. 80NSSC18K0849 issued through the Planetary Astronomy Program. This work was supported by the National Science Centre, Poland, through grant no. 2014/13/D/ST9/01818 (A.M.). The research leading to these results has received funding from the European Union's Horizon 2020 Research and Innovation Programme, under Grant Agreement no 687 378 (SBNAF). This project has been supported by the GINOP-2.3.2-15-2016-00003 and NKFIH K125015 grants of the Hungarian National Research, Development and Innovation Office (NKFIH) and by the Lendület grant LP2012-31 of the Hungarian Academy of Sciences. TRAPPIST-North is a project funded by the University of Liège, in collaboration with Cadi Ayyad University of Marrakech (Morocco). TRAPPIST-South is a project funded by the Belgian FNRS under grant FRFC 2.5.594.09. F.E.J. is a FNRS Senior Research Associate. ASAS-SN thanks the Las Cumbres Observatory and its staff for its continuing support of the ASAS-SN project. ASAS-SN is supported by the Gordon and Betty Moore Foundation through grant GBMF5490 to the Ohio State University and NSF grant AST-1515927. Development of ASAS-SN has been supported by NSF grant AST-0908816, the Mt. Cuba Astronomical Foundation, the Center for Cosmology and AstroParticle Physics at the Ohio State University, the Chinese Academy of Sciences South America Center for Astronomy (CASSACA), the Villum Foundation, and George Skestos.

References

Baer, J., & Chesley, S. R. 2008, Celest. Mech. Dyn. Astron., 100, 27
Baer, J., & Chesley, S. R. 2017, AJ, 154, 76
Baer, J., Chesley, S. R., & Matson, R. D. 2011, AJ, 141, 143
Carry, B. 2012, Planet. Space Sci., 73, 98
Carry, B., Kaasalainen, M., Merline, W. J., et al. 2012, Planet. Space Sci., 66, 200
Carry, B., Vachier, F., Berthier, J., et al. 2019, A&A, 623, A132
Chambat, F., Ricard, Y., & Valette, B. 2010, Geophys. J. Int., 183, 727
Chandrasekhar, S. 1969, Ellipsoidal Figures of Equilibrium (New Haven, USA: Yale University Press)
Chernetenko, Y. A., & Kochetova, O. M. 2002, ESA SP, 500, 437
Clark, B. E., Ziffer, J., Nesvorny, D., et al. 2010, J. Geophys. Res. Planets, 115, E06005
Conrad, A. R., Dumas, C., Merline, W. J., et al. 2007, Icarus, 191, 616
De Angelis, G. 1995, Planet. Space Sci., 43, 649
Dermott, S. F. 1979, Icarus, 37, 575
Drummond, J., & Christou, J. 2008, Icarus, 197, 480
Drummond, J., Christou, J., & Nelson, J. 2009, Icarus, 202, 147
Ďurech, J., & Hanuš, J. 2018, A&A, 620, A91
Ďurech, J., Kaasalainen, M., Warner, B. D., et al. 2009, A&A, 493, 291
Ďurech, J., Sidorin, V., & Kaasalainen, M. 2010, A&A, 513, A46
Ďurech, J., Hanuš, J., Oszkiewicz, D., & Vančo, R. 2016, A&A, 587, A48
Fétick, R. J., Jorda, L., Vernazza, P., et al. 2019, A&A, 623, A6
Fienga, A., Laskar, J., Morley, T., et al. 2009, A&A, 507, 1675
Fienga, A., Kuchynka, P., Laskar, J., Manche, H., & Gastineau, M. 2011, EPSC-DPS Joint Meeting 2011, 1879
Fienga, A., Manche, H., Laskar, J., Gastineau, M., & Verma, A. 2013, ArXiv e-prints [arXiv:1301.1510]
Fienga, A., Manche, H., Laskar, J., Gastineau, M., & Verma, A. 2014, ArXiv e-prints [arXiv:1405.0484]
Folkner, W. M., Williams, J. G., & Boggs, D. H. 2009, IPN Prog. Rep., 42, 1
Fujiwara, A., Kawaguchi, J., Yeomans, D. K., et al. 2006, Science, 312, 1330
Gaia Collaboration (Spoto, F., et al.) 2018, A&A, 616, A13
Goffin, E. 2014, A&A, 565, A56
Grice, J., Snodgrass, C., Green, S. F., Parley, N. R., & Carry, B. 2017, in Asteroids, Comets, and Meteors: ACM 2017 (Mankato, USA: Capstone Publishers)
Hanuš, J., Ďurech, J., Brož, M., et al. 2011, A&A, 530, A134
Hanuš, J., Ďurech, J., Brož, M., et al. 2013, A&A, 551, A67
Hanuš, J., Viikinkoski, M., Marchis, F., et al. 2017, A&A, 601, A114
Hanuš, J., Vokrouhlický, D., Delbo', M., et al. 2018, A&A, 620, L8
Hanuš, J., Marsset, M., Vernazza, P., et al. 2019, A&A, 624, A121
Hiesinger, H., Marchi, S., Schmedemann, N., et al. 2016, Science, 353, 4758
Hubbard, W. B. 2013, ApJ, 768, 43
Ivantsov, A. 2008, Planet. Space Sci., 56, 1857
Jehin, E., Gillon, M., Queloz, D., et al. 2011, The Messenger, 145, 2
Kaasalainen, M., & Torppa, J. 2001, Icarus, 153, 24
Kaasalainen, M., Torppa, J., & Muinonen, K. 2001, Icarus, 153, 37
Kochanek, C. S., Shappee, B. J., Stanek, K. Z., et al. 2017, PASP, 129, 104502
Kochetova, O. M. 2004, Sol. Syst. Res., 38, 66
Kochetova, O. M., & Chernetenko, Y. A. 2014, Sol. Sys. Res., 48, 295
Konopliv, A. S., Asmar, S. W., Folkner, W. M., et al. 2011, Icarus, 211, 401
Kopal, S. 1960, Figures of Equilibrium of Celestial Bodies (Madison, USA: University of Wisconsin Press)

Krasinsky, G. A., Pitjeva, E. V., Vasiliev, M. V., & Yagudina, E. I. 2001, Commun. IAA RAS, 6, 114
Kuchynka, P., & Folkner, W. M. 2013, Icarus, 222, 243
Landgraf, W. 1992, IAU Symp., 152, 179
Lanzano, P. 1974, Ap&SS, 29, 161
Lustig, G., & Hahn, G. 1976, Acta Phys. Austriaca, 44, 199
Marciniak, A., Pilcher, F., Oszkiewicz, D., et al. 2015, Planet. Space Sci., 118, 256
Marsset, M., Vernazza, P., Birlan, M., et al. 2016, A&A, 586, A15
Marsset, M., Carry, B., Dumas, C., et al. 2017, A&A, 604, A64
Masiero, J. R., Mainzer, A. K., Bauer, J. M., et al. 2013, ApJ, 770, 7
Masiero, J. R., Grav, T., Mainzer, A. K., et al. 2014, ApJ, 791, 121
Merline, W. J., Drummond, J. D., Carry, B., et al. 2013, Icarus, 225, 794
Michalak, G. 2001, A&A, 374, 703
Michalowski, T. 1993, Icarus, 106, 563
Michalowski, T., Velichko, F. P., Di Martino, M., et al. 1995, Icarus, 118, 292
Moritz, H. 1990, The Figure of the Earth : Theoretical Geodesy and the Earth's Interior (Heidelberg, Germany: Wichmann)
Müller, T. G., Marciniak, A., Kiss, C., et al. 2018, Adv. Space Res., 62, 2326
Nolan, M. C., Magri, C., Howell, E. S., et al. 2013, Icarus, 226, 629
Park, R., Konopliv, A., Bills, B., et al. 2016, EGU General Assembly Conf. Abstracts, 18, 8395
Park, R. S., Vaughan, A. T., Konopliv, A. S., et al. 2019, Icarus, 319, 812
Piironen, J., Lagerkvist, C., Torppa, J., Kaasalainen, M., & Warner, B. 2001, BAAS, 33, 1562
Pitjeva, E. V. 2013, Sol. Syst. Res., 47, 386
Rambaux, N., Chambat, F., & Castillo-Rogez, J. C. 2015, A&A, 584, A127
Rambaux, N., Baguet, D., Chambat, F., & Castillo-Rogez, J. C. 2017, ApJ, 850, L9
Rivkin, A. S., Howell, E. S., & Emery, J. P. 2019, J Geophys. Res. Planets, 124, 1393
Rubincam, D. P. 2000, Icarus, 148, 2
Satō, I., Buie, M., Maley, P. D., et al. 2014, Int. J. Astron. Astrophys., 4, 91
Ševeček, P., Brož, M., & Jutzi, M. 2019, A&A, 629, A122
Shappee, B. J., Prieto, J. L., Grupe, D., et al. 2014, ApJ, 788, 48
Shevchenko, V. G., Chernyi, V. G., Kruglyi, I. N., et al. 1992, Icarus, 100, 295
Siltala, L., & Granvik, M. 2017, Icarus, 297, 149
Somenzi, L., Fienga, A., Laskar, J., & Kuchynka, P. 2010, Planet. Space Sci., 58, 858
Takir, D., & Emery, J. P. 2012, Icarus, 219, 641
Tempesti, P. 1975, Mem. Soc. Astron. It., 46, 397
Thalmann, C., Schmid, H. M., Boccaletti, A., et al. 2008, Proc. SPIE, 7014, 70143F
Usui, F., Hasegawa, S., Ootsubo, T., & Onaka, T. 2019, PASJ, 71, 1
Vasiliev, M. V., & Yagudina, E. I. 1999, Commun. IAA RAS, 4, 98
Vernazza, P., Marsset, M., Beck, P., et al. 2015, ApJ, 806, 204
Vernazza, P., Castillo-Rogez, J., Beck, P., et al. 2017, AJ, 153, 72
Vernazza, P., Brož, M., Drouard, A., et al. 2018, A&A, 618, A154
Vernazza, P., Jorda, L., Ševeček, P., et al. 2019, Nat. Astron., in press, http://doi.org/10.1038/s41550-019-0915-8
Veverka, J., Robinson, M., Thomas, P., et al. 2000, Meteorit. Planet. Sci., 35, 164
Viikinkoski, M., Kaasalainen, M., & Ďurech, J. 2015a, A&A, 576, A8
Viikinkoski, M., Kaasalainen, M., Ďurech, J., et al. 2015b, A&A, 581, L3
Viikinkoski, M., Hanuš, J., Kaasalainen, M., Marchis, F., & Ďurech, J. 2017, A&A, 607, A117
Viikinkoski, M., Vernazza, P., Hanuš, J., et al. 2018, A&A, 619, L3
Viswanathan, V., Fienga, A., Gastineau, M., & Laskar, J. 2017, Notes Scientifiques et Techniques de l'Institut de mécanique céleste, (ISSN 1621-3823), 108, 39
Vokrouhlický, D., Nesvorný, D., & Bottke, W. F. 2003, Nature, 425, 147
Warner, B. D. 2018, Minor Planet Bull., 45, 39
Watanabe, S., Hirabayashi, M., Hirata, N., et al. 2019, Science, 364, 268
Yang, X.-Y., Zhang, Y.-Y., & Li, X.-Q. 1965, Acta Astron. Sin., 13, 66
Zielenbach, W. 2011, AJ, 142, 120

[1] Institute of Astronomy, Faculty of Mathematics and Physics, Charles University, V Holešovičkách 2, 18000 Prague, Czech Republic
e-mail: pepa@sirrah.troja.mff.cuni.cz

[2] Aix Marseille Univ, CNRS, LAM, Laboratoire d'Astrophysique de Marseille, Marseille, France
[3] Mathematics and Statistics, Tampere University, 33720 Tampere, Finland
[4] Space sciences, Technologies and Astrophysics Research Institute, Université de Liège, Allée du 6 Août 17, 4000 Liège, Belgium
[5] IMCCE, Observatoire de Paris, 77 avenue Denfert-Rochereau, 75014 Paris Cedex, France
[6] Astronomical Observatory Institute, Faculty of Physics, Adam Mickiewicz University, ul. Słoneczna 36, 60-286 Poznań, Poland
[7] Université Côte d'Azur, Observatoire de la Côte d'Azur, CNRS, Laboratoire Lagrange, France
[8] Department of Earth, Atmospheric and Planetary Sciences, MIT, 77 Massachusetts Avenue, Cambridge, MA 02139, USA
[9] SETI Institute, Carl Sagan Center, 189 Bernado Avenue, Mountain View CA 94043, USA
[10] Center for Solar System Studies, 446 Sycamore Ave., Eaton, CO 80615, USA
[11] Geneva Observatory, 1290 Sauverny, Switzerland
[12] Asociación Astronómica Astro Henares, Centro de Recursos Asociativos El Cerro C/ Manuel Azaña, 28823 Coslada, Madrid, Spain
[13] 490 chemin du Gonnet, 38440 Saint Jean de Bournay, France
[14] Institute of Geology, A. Mickiewicz University, Krygowskiego 12, 61-606 Poznań, Poland
[15] Observatoire de Durtal, 49430 Durtal, France
[16] Observatorio Astronómico de Córdoba, Córdoba, Argentina
[17] 20 parc des Pervenches, 13012 Marseille, France
[18] Instituto de Astrofisica de Andalucia – CSIC. Glorieta de la Astronomía s/n, 18008 Granada, Spain
[19] I64, SL6 1XE Maidenhead, UK
[20] Uranoscope, Avenue Carnot 7, 77220 Gretz-Armainvilliers, France
[21] Anunaki Observatory, Calle de los Llanos, 28410 Manzanares el Real, Spain
[22] Departamento de Astrofisica, Universidad de La Laguna, 38206 La Laguna, Tenerife, Spain
[23] Institute of Theoretical Physics, Faculty of Mathematics and Physics, Charles University, V Holešovičkách 2, 18000 Prague, Czech Republic
[24] Courbes de rotation d'astéroïdes et de comètes, CdR, Geneva Observatory, 1290 Sauverny, Switzerland
[25] Institute for Astronomy, University of Hawai'i, 2680 Woodlawn Drive, Honolulu, HI 96822, USA
[26] Observatorio Amanecer de Arrakis, Alcalá de Guadaíra, Sevilla, Spain
[27] Konkoly Observatory, Research Centre for Astronomy and Earth Sciences, Hungarian Academy of Sciences, Konkoly Thege 15-17, 1121 Budapest, Hungary
[28] Thirty-Meter-Telescope, 100 West Walnut St, Suite 300, Pasadena, CA 91124, USA
[29] Jet Propulsion Laboratory, California Institute of Technology, 4800 Oak Grove Drive, Pasadena, CA 91109, USA
[30] European Space Agency, ESTEC – Scientific Support Office, Keplerlaan 1, Noordwijk 2200 AG, The Netherlands
[31] Open University, School of Physical Sciences, The Open University, MK7 6AA, UK
[32] Laboratoire Atmosphères, Milieux et Observations Spatiales, CNRS & UVSQY, Guyancourt, France
[33] Departamento de Física, Ingeniería de Sistemas y Teoría de la Señal, Universidad de Alicante, 03080 Alicante, Spain
[34] Institut de Ciències del Cosmos, Universitat de Barcelona (IEEC-UB), Martí i Franquès 1, 08028 Barcelona, Spain
[35] European Southern Observatory (ESO), Alonso de Cordova 3107, 1900 Casilla Vitacura, Santiago, Chile

Appendix A: Additional figures and tables

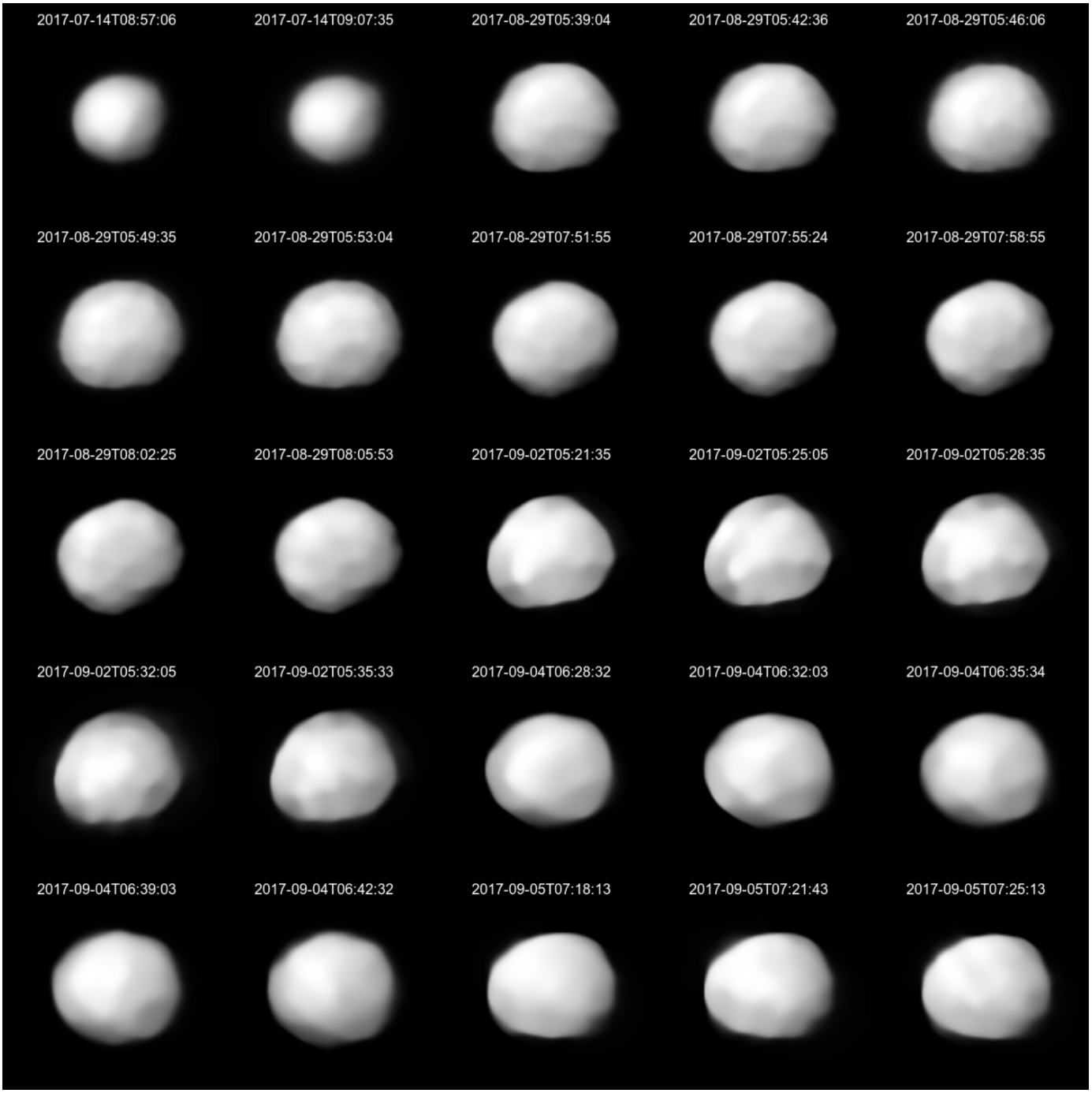

Fig. A.1. Full set of VLT/SPHERE/ZIMPOL images of (704) Interamnia obtained in August–September 2017. All images were deconvolved with the `Mistral` algorithm. Table A.1 contains full information about the data.

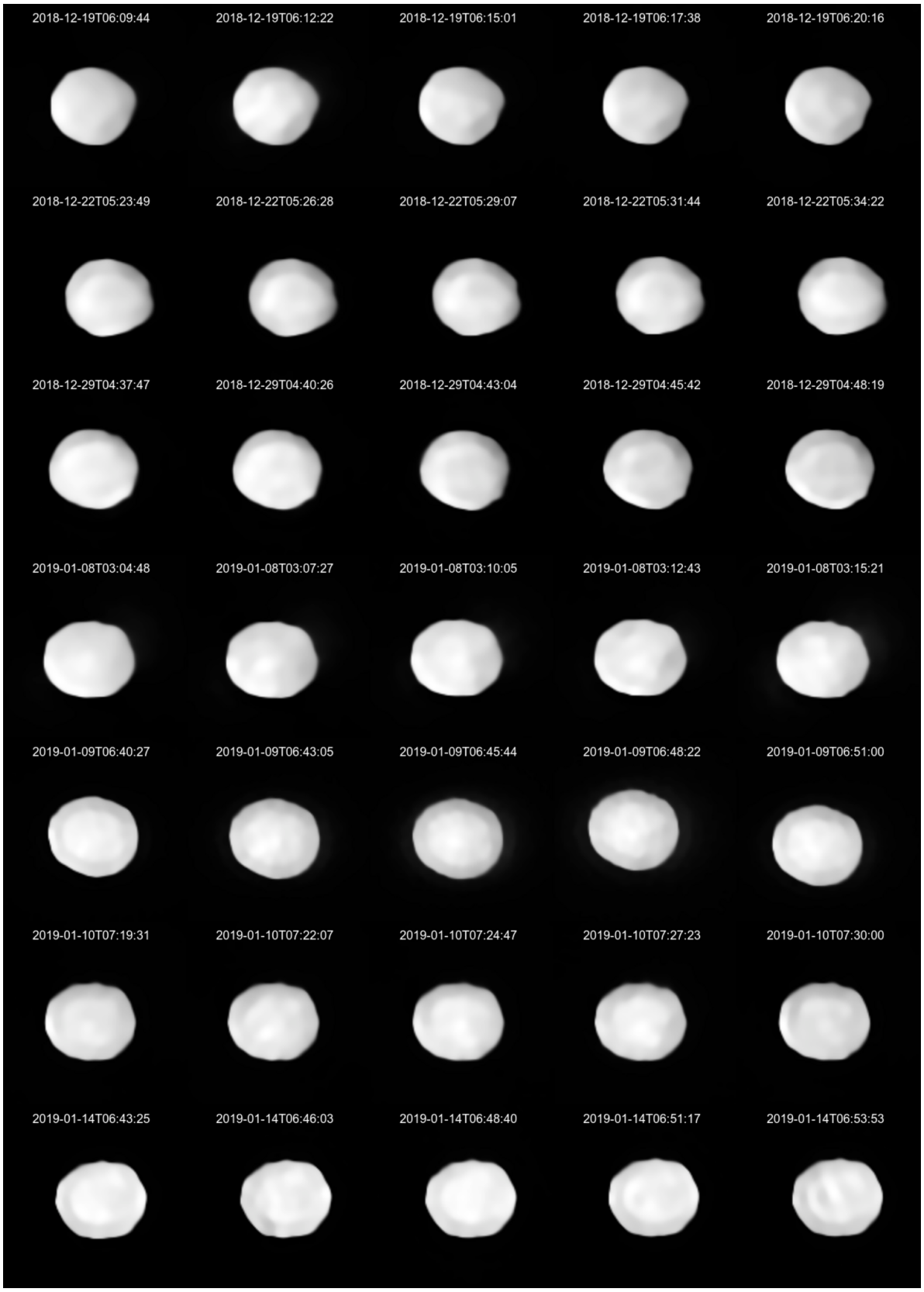

Fig. A.2. Full set of VLT/SPHERE/ZIMPOL images of (704) Interamnia obtained between December 2018 and January 2019. All images were deconvolved with the `Mistral` algorithm. Table A.1 contains full information about the data.

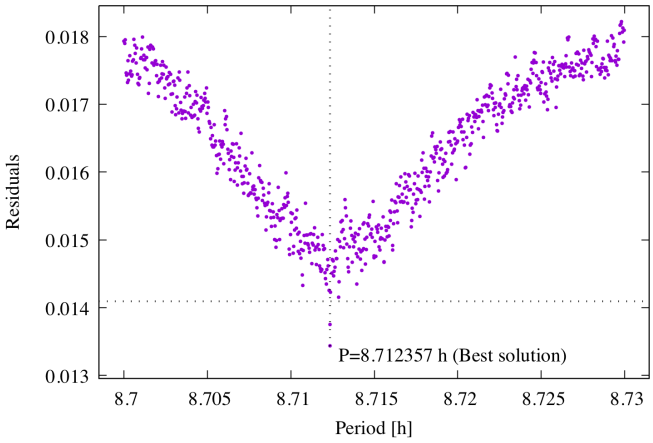

Fig. A.3. Periodogram for Interamnia: each point corresponds to a local minimum in the parameter space. The point with the lowest rms is the global minimum and the horizontal line indicates the rms threshold as defined in Hanuš et al. (2018).

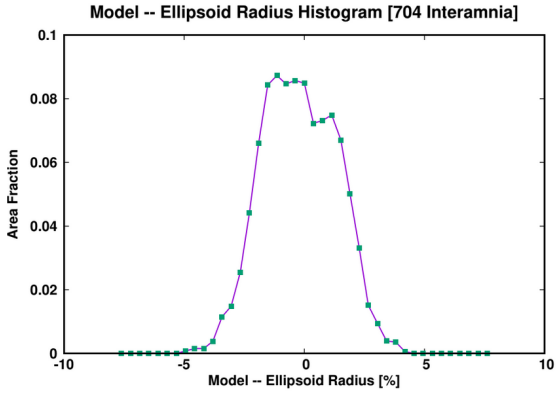

Fig. A.5. Distribution of residuals measured along the local normal direction between the ADAM shape model and the best-fitting ellipsoid.

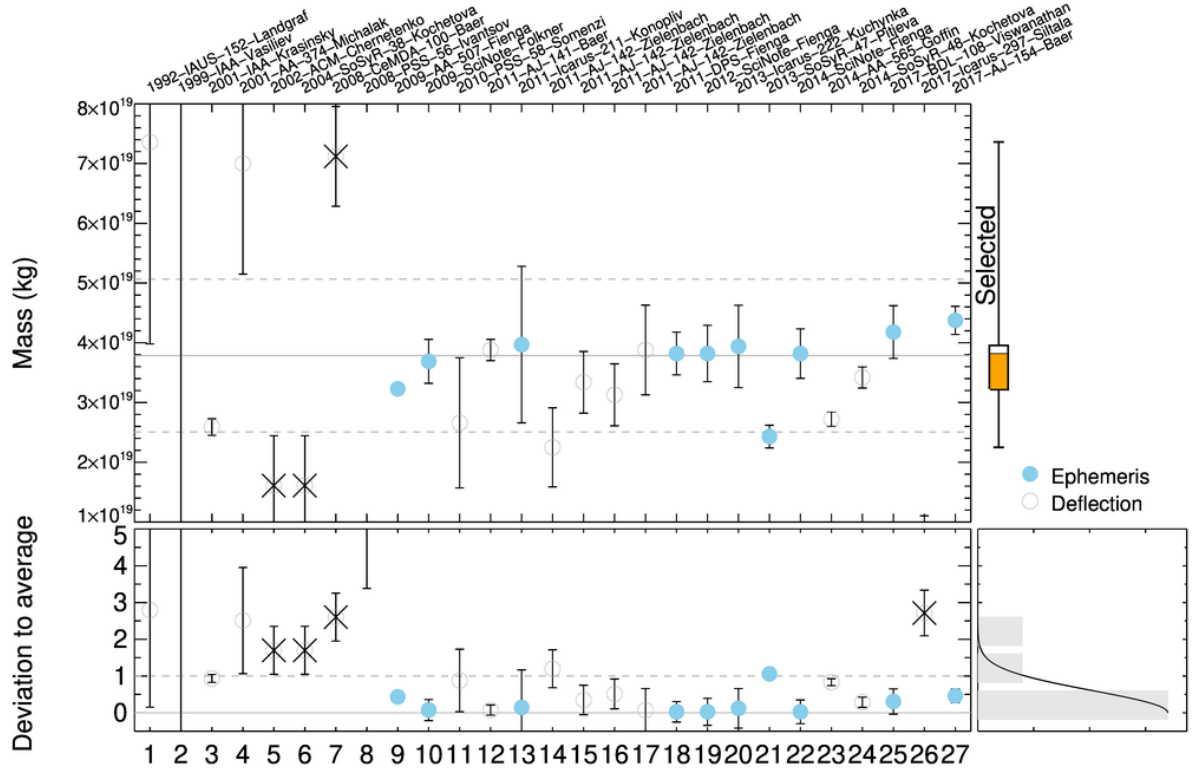

Fig. A.4. Mass estimates ($\mathcal{M}$) of (704) Interamnia collected in the literature.

Table A.1. VLT/SPHERE disk-resolved images obtained in the I filter by the ZIMPOL camera.

Date	UT	Exp (s)	Airmass	Δ (AU)	r (AU)	α (°)	D_a (″)
2017-07-14	8:57:06	200	1.46	2.24	2.62	22.4	0.203
2017-07-14	9:07:35	200	1.45	2.24	2.62	22.4	0.203
2017-08-29	5:39:04	200	1.71	1.78	2.60	15.9	0.256
2017-08-29	5:42:36	200	1.70	1.78	2.60	15.9	0.256
2017-08-29	5:46:06	200	1.70	1.78	2.60	15.9	0.256
2017-08-29	5:49:35	200	1.69	1.78	2.60	15.9	0.256
2017-08-29	5:53:04	200	1.69	1.78	2.60	15.9	0.256
2017-08-29	7:51:55	200	1.88	1.78	2.60	15.9	0.256
2017-08-29	7:55:24	200	1.89	1.78	2.60	15.9	0.256
2017-08-29	7:58:55	200	1.91	1.78	2.60	15.9	0.256
2017-08-29	8:02:25	200	1.93	1.78	2.60	15.9	0.256
2017-08-29	8:05:53	200	1.95	1.78	2.60	15.9	0.256
2017-09-02	5:21:35	200	1.72	1.76	2.60	15.0	0.259
2017-09-02	5:25:05	200	1.71	1.76	2.60	15.0	0.259
2017-09-02	5:28:35	200	1.71	1.76	2.60	15.0	0.259
2017-09-02	5:32:05	200	1.70	1.76	2.60	15.0	0.259
2017-09-02	5:35:33	200	1.70	1.76	2.60	15.0	0.259
2017-09-04	6:28:32	200	1.72	1.74	2.60	14.5	0.261
2017-09-04	6:32:03	200	1.73	1.74	2.60	14.5	0.261
2017-09-04	6:35:34	200	1.73	1.74	2.60	14.5	0.261
2017-09-04	6:39:03	200	1.74	1.74	2.60	14.5	0.261
2017-09-04	6:42:32	200	1.75	1.74	2.60	14.5	0.261
2017-09-05	7:18:13	200	1.89	1.74	2.60	14.3	0.261
2017-09-05	7:21:43	200	1.91	1.74	2.60	14.3	0.261
2017-09-05	7:25:13	200	1.92	1.74	2.60	14.3	0.261
2018-12-19	6:09:44	147	1.35	2.15	3.02	10.1	0.212
2018-12-19	6:12:22	147	1.35	2.15	3.02	10.1	0.212
2018-12-19	6:15:01	147	1.34	2.15	3.02	10.1	0.212
2018-12-19	6:17:38	147	1.34	2.15	3.02	10.1	0.212
2018-12-19	6:20:16	147	1.34	2.15	3.02	10.1	0.212
2018-12-22	5:23:49	147	1.41	2.13	3.03	9.2	0.214
2018-12-22	5:26:28	147	1.40	2.13	3.03	9.2	0.214
2018-12-22	5:29:07	147	1.39	2.13	3.03	9.2	0.214
2018-12-22	5:31:44	147	1.39	2.13	3.03	9.2	0.214
2018-12-22	5:34:22	147	1.38	2.13	3.03	9.2	0.214
2018-12-29	4:37:47	147	1.43	2.10	3.04	6.7	0.217
2018-12-29	4:40:26	147	1.43	2.10	3.04	6.7	0.217
2018-12-29	4:43:04	147	1.42	2.10	3.04	6.7	0.217
2018-12-29	4:45:42	147	1.41	2.10	3.04	6.7	0.217
2018-12-29	4:48:19	147	1.40	2.10	3.04	6.7	0.217
2019-01-08	3:04:48	147	1.60	2.08	3.05	3.3	0.219
2019-01-08	3:07:27	147	1.59	2.08	3.05	3.3	0.219
2019-01-08	3:10:05	147	1.58	2.08	3.05	3.3	0.219
2019-01-08	3:12:43	147	1.56	2.08	3.05	3.3	0.219
2019-01-08	3:15:21	147	1.55	2.08	3.05	3.3	0.219
2019-01-09	6:40:27	147	1.42	2.08	3.05	2.9	0.219
2019-01-09	6:43:05	147	1.43	2.08	3.05	2.9	0.219
2019-01-09	6:45:44	147	1.44	2.08	3.05	2.9	0.219
2019-01-09	6:48:22	147	1.44	2.08	3.05	2.9	0.219
2019-01-09	6:51:00	147	1.45	2.08	3.05	2.9	0.219
2019-01-10	7:19:31	147	1.59	2.08	3.06	2.6	0.219
2019-01-10	7:22:07	147	1.61	2.08	3.06	2.6	0.219
2019-01-10	7:24:47	147	1.62	2.08	3.06	2.6	0.219
2019-01-10	7:27:23	147	1.64	2.08	3.06	2.6	0.219
2019-01-10	7:30:00	147	1.65	2.08	3.06	2.6	0.219
2019-01-14	6:43:25	147	1.51	2.08	3.06	2.0	0.219
2019-01-14	6:46:03	147	1.52	2.08	3.06	2.0	0.219
2019-01-14	6:48:40	147	1.53	2.08	3.06	2.0	0.219
2019-01-14	6:51:17	147	1.55	2.08	3.06	2.0	0.219
2019-01-14	6:53:53	147	1.56	2.08	3.06	2.0	0.219

Notes. For each observation, the table gives the epoch, the exposure time, the airmass, the distance to the Earth Δ and the Sun r, the phase angle α, and the angular diameter D_a.

Table A.2. Stellar occultations used for shape modeling, with individual observers names.

(704) Interamnia
1996-12-17
Bob Fried, Braeside Obs., Flagstaff, AZ, USA
Gary Goodman, Camarillo, CA, USA
Etscorn Obs., Socorro, NM, USA
Orange County A.S. Obs., Anza, CA, USA
F. Wright/Fulton Jr., Prescott, AZ, USA
Pierre Schwaar, Phoenix, AZ, USA
P. Maley/L Paller, Phoenix, AZ, USA
Sam Herchak, Mesa, AZ, USA
Table Mtn. Obs., Wrightwood, CA, USA
Ken Ziegler, Gila Obs., Globe, AZ, USA
Bill Peters, AZ, USA
2003-3-23
Yoshida Hidetoshi, Abashiri, Hokkaido, JP
Kouda Masaki, Kamikita, Aomori, JP
Imatani & Takashi, Kitaura, Ibaraka, JP
Sugawara Hitoshi, Ichinoseki, Iwate, JP
Satou Toshirou, Ichinoseki, Iwate, JP
Yokokawa Mikio, Motoyoshi, Miyagi, JP
Konno Eitoshi, Hanaizumi, Iwate JP
Sasaki Kazuo, Furukawa, Miyagi, JP
Tonomura Yasuhiro, Tomiya, Miyagi, JP
Okamoto Michiko, Rifu, Miyagi, JP
Sakaki Chiyoaki, Sendai, Miyagi, JP
Nagai Hideo, Sendai, Miyagi, JP
Itou Yoshiharu, Aoba, Sendai, JP
Ikeshita Ryo et al., Kawauchi, Sendai, JP
Koishikawa Masahiro, Sendai, Miyagi, JP
Watanabe, Akira, Sendai, Miyagi, JP
Miyamoto Atsushi et al, Adachi, JP
Sugai Hideo, Zao-hango, Yamagata, JP
Fujita Mitsuhiro, Shiroishi, Miyagi, JP
Nihei Hajime, Nanyo, Yamagata, JP
Tanaka Takashi, Zushi, Kanagawa, JP
Sato Tsutomu, Marumori, Miyagi, JP
Ootsuki Isao, Marumori, Miyagi, JP
David Tholen, Turtle Bay, Oahu, Hawaii, USA
Sato Hikaru, Fukushima, JP
Sato Makoto, Haranomachi, Fukushima, JP
Rebecca Sydney, Honolua Bay, Maui, HI
Bedient et al., Foster Village, Hawaii, USA
Hamanowa et al., Koriyama City, JP
Usuki Ken-ichi, Niitsuru, Fukushima, JP
Lewis Roberts, Haleakala, Hawaii, USA
Watanabe et al., Takine, Fukushima, JP
Sato Hirohisa, Sukagawa, Fukushima, JP
David Dunham, Makena, Maui, HI, USA
B. Brevoort, Hawaii, USA
Tsuchikawa Akira, Yanagida, JP
S. Bus, Mauna Kea, Hawaii, USA
R. Savalle, Mauna Kea, Hawaii, USA
Tomioka Hiroyuki, Hitachi, Ibaraki, JP
P. Maley, Hawaii, USA
Yaeza Akira,Moriyama-cho, Hitachi, JP
E. Cleintuar, Hawaii, USA
S. O'Meara, Mauna Loa, USA
W. Fukunaga, Hawaii, USA
V. Fukunaga, Hawaii, USA
J. Swatek, Hawaii, USA
Uehara Sadaharu, Ibaraki, JP
Observer
Kuboniwa Atasushi, Ushika,Ibaraka, JP
Kita Nobusuke, Kashiwa, Chiba, JP
Takashima et al, Kashiwa, Chiba, JP
Momose Masahiko, Shiojiri, Nagano, JP
Kaneko Sakae, Sakura, Chiba, JP
Nakanishi Akio, Itabashi, Tokyo, JP
Ishida Masayuki, Kanazu, Fukui, JP
Kitazaki Katsuhiko, Tokyo, JP
Ida Miyoshi, Muraoka, Fukui, JP
Suzuki Satoshi, Yokohama,Kanagawa, JP
Hirose Yoji, Chigasaki, Kanagawa, JP
Sugiyama Yukihiro, Hiratsuka, JP
Yoneyama Seiichi, Ogaki, Gifu, JP
Oribe Takaaki et al., Saji, Tottori, JP
2007-9-9
R. Cadmus, Grinnell, IA, USA
J. Centala, Marion, IA, USA
W. Osborn/C. Tycner, Mt. Pleasant, MI, USA
P. Maley, Bernalillo, NM, USA
K. McKeown, Los Lunas, NM, USA
D. Dunham, Dubuque IA, USA
2012-11-12
N. Smith, Trenton, GA, USA
T. Blank/M. Pacht, Taftsville, VT, USA
S. Conard, Gamber, MD, USA
A. Scheck, Scaggsville, MD, USA
C. Ellington, Owings, MD, USA

Table A.3. Optical disk-integrated lightcurves used for ADAM shape modeling.

N	Epoch	N_p	Δ (AU)	r (AU)	φ (°)	Filter	Reference
1	1964-11-22.7	81	1.82	2.75	8.1	*V*	Yang et al. (1965)
2	1964-11-23.7	57	1.81	2.75	7.7	*V*	Yang et al. (1965)
3	1969-08-16.5	8	2.18	2.58	22.6	*V*	Tempesti (1975)
4	1969-08-20.6	7	2.14	2.58	22.3	*V*	Tempesti (1975)
5	1969-08-21.5	12	2.13	2.58	22.2	*V*	Tempesti (1975)
6	1969-09-08.5	12	1.95	2.59	19.9	*V*	Tempesti (1975)
7	1969-10-05.6	13	1.74	2.60	13.9	*V*	Tempesti (1975)
8	1969-10-15.4	10	1.70	2.60	11.4	*V*	Tempesti (1975)
9	1969-11-01.4	11	1.68	2.61	9.1	*V*	Tempesti (1975)
10	1969-11-03.4	15	1.68	2.61	9.2	*V*	Tempesti (1975)
11	1969-11-10.5	23	1.69	2.62	9.8	*V*	Tempesti (1975)
12	1974-08-27.1	29	1.71	2.62	12.2	*V*	Lustig & Hahn (1976)
13	1974-08-28.0	91	1.71	2.62	12.1	*V*	Lustig & Hahn (1976)
14	1974-08-29.0	92	1.71	2.62	11.9	*V*	Lustig & Hahn (1976)
15	1990-08-01.9	76	1.86	2.68	15.5	*V*	Shevchenko et al. (1992)
16	1993-03-21.6	77	2.55	3.47	7.6	*V*	Michalowski et al. (1995)
17	1993-03-23.6	73	2.56	3.47	7.9	*V*	Michalowski et al. (1995)
18	1996-12-13.2	512	1.83	2.74	9.6	*V*	Satō et al. (2014)
19	1996-12-13.3	354	1.83	2.74	9.6	*R*	Satō et al. (2014)
20	2003-03-31.9	29	2.85	3.20	17.8	*C*	Stephane Charbonnel
21	2003-03-31.9	55	2.85	3.20	17.8	*C*	Nathanal Berger
22	2006-06-04.1	30	2.46	2.79	21.0	*C*	Arnaud Leroy
23	2006-07-21	59	1.89	2.74	14.3	*C*	Grice et al. (2017)
24	2006-07-25	53	1.86	2.73	13.3	*C*	Grice et al. (2017)
25	2006-07-25	54	1.86	2.73	13.3	*C*	Grice et al. (2017)
26	2006-07-26	38	1.85	2.73	13.1	*C*	Grice et al. (2017)
27	2006-07-26	40	1.85	2.73	13.1	*C*	Grice et al. (2017)
28	2006-07-27	50	1.85	2.73	12.8	*C*	Grice et al. (2017)
29	2006-07-27	55	1.85	2.73	12.8	*C*	Grice et al. (2017)
30	2006-07-28	56	1.84	2.73	12.6	*C*	Grice et al. (2017)
31	2006-07-28	56	1.84	2.73	12.6	*C*	Grice et al. (2017)
32	2006-07-29	54	1.83	2.73	12.3	*C*	Grice et al. (2017)
33	2006-07-29	58	1.83	2.73	12.3	*C*	Grice et al. (2017)
34	2006-07-30	59	1.82	2.72	12.1	*C*	Grice et al. (2017)
35	2006-07-30	59	1.82	2.72	12.1	*C*	Grice et al. (2017)
36	2006-07-31	46	1.82	2.72	11.8	*C*	Grice et al. (2017)
37	2006-07-31	59	1.82	2.72	11.8	*C*	Grice et al. (2017)
38	2006-08-02	64	1.81	2.72	11.3	*C*	Grice et al. (2017)
39	2006-08-04	89	1.79	2.72	10.8	*C*	Grice et al. (2017)
40	2006-08-05	51	1.79	2.72	10.6	*C*	Grice et al. (2017)
41	2006-08-05	87	1.79	2.72	10.6	*C*	Grice et al. (2017)
42	2006-08-06	61	1.78	2.72	10.3	*C*	Grice et al. (2017)
43	2006-08-06	89	1.78	2.72	10.3	*C*	Grice et al. (2017)
44	2006-08-07	62	1.78	2.72	10.1	*C*	Grice et al. (2017)
45	2006-08-07	88	1.78	2.72	10.1	*C*	Grice et al. (2017)
46	2006-08-12	105	1.76	2.71	9.0	*C*	Grice et al. (2017)
47	2006-08-12	118	1.76	2.71	9.0	*C*	Grice et al. (2017)
48	2006-08-13	67	1.75	2.71	8.9	*C*	Grice et al. (2017)
49	2006-08-13	91	1.75	2.71	8.9	*C*	Grice et al. (2017)
50	2006-08-19	49	1.74	2.70	8.1	*C*	Grice et al. (2017)
51	2006-08-20	41	1.74	2.70	8.0	*C*	Grice et al. (2017)
52	2006-08-22	54	1.73	2.70	7.9	*C*	Grice et al. (2017)
53	2006-08-25	42	1.73	2.70	8.0	*C*	Grice et al. (2017)
54	2006-08-30	52	1.73	2.69	8.4	*C*	Grice et al. (2017)
55	2006-08-31	67	1.73	2.69	8.5	*C*	Grice et al. (2017)

Notes. For each lightcurve, the table gives the epoch, the number of individual measurements N_p, asteroid's distances to the Earth Δ and the Sun r, phase angle φ, photometric filter and observation information. *Gaia*-GOSA (*Gaia*-Ground-based Observational Service for Asteroids, www.gaiagosa.eu).

Table A.3. continued.

N	Epoch	N_p	Δ (AU)	r (AU)	φ (°)	Filter	Reference
56	2006-08-32.0	236	1.73	2.69	8.5	*C*	Dominique Suys, Hugo Riemis, Jan Vantomme
57	2006-09-02	52	1.74	2.69	8.9	*C*	Grice et al. (2017)
58	2006-09-12	57	1.77	2.68	11.1	*C*	Grice et al. (2017)
59	2006-09-14	50	1.77	2.68	11.6	*C*	Grice et al. (2017)
60	2006-09-16	46	1.78	2.68	12.1	*C*	Grice et al. (2017)
61	2006-09-19	38	1.80	2.67	12.9	*C*	Grice et al. (2017)
62	2006-09-22	46	1.82	2.67	13.7	*C*	Grice et al. (2017)
63	2006-09-24	47	1.83	2.67	14.3	*C*	Grice et al. (2017)
64	2006-09-26	47	1.84	2.67	14.8	*C*	Grice et al. (2017)
65	2006-09-27	38	1.85	2.67	15.0	*C*	Grice et al. (2017)
66	2006-10-08	43	1.94	2.66	17.6	*C*	Grice et al. (2017)
67	2007-10-18	39	2.29	2.78	19.8	*C*	Grice et al. (2017)
68	2007-11-22	80	1.96	2.82	11.7	*C*	Grice et al. (2017)
69	2007-12-27.9	34	1.90	2.87	3.1	*C*	Jean-Francois Coliac
70	2008-12-28	58	2.94	3.37	16.2	*C*	Grice et al. (2017)
71	2009-01-03	59	2.87	3.37	15.5	*C*	Grice et al. (2017)
72	2009-01-04	58	2.85	3.38	15.4	*C*	Grice et al. (2017)
73	2009-01-17	61	2.71	3.39	13.5	*C*	Grice et al. (2017)
74	2009-01-18	55	2.70	3.39	13.4	*C*	Grice et al. (2017)
75	2009-01-20	53	2.68	3.39	13.0	*C*	Grice et al. (2017)
76	2009-01-20	73	2.68	3.39	13.0	*C*	Grice et al. (2017)
77	2009-01-21	58	2.67	3.39	12.8	*C*	Grice et al. (2017)
78	2009-01-23	51	2.65	3.39	12.4	*C*	Grice et al. (2017)
79	2009-01-24	55	2.65	3.39	12.2	*C*	Grice et al. (2017)
80	2009-01-24	77	2.64	3.39	12.2	*C*	Grice et al. (2017)
81	2009-01-25	56	2.64	3.40	12.0	*C*	Grice et al. (2017)
82	2009-01-26	61	2.63	3.40	11.8	*C*	Grice et al. (2017)
83	2009-01-27	71	2.62	3.40	11.6	*C*	Grice et al. (2017)
84	2009-01-28	73	2.61	3.40	11.4	*C*	Grice et al. (2017)
85	2009-01-31	60	2.59	3.40	10.8	*C*	Grice et al. (2017)
86	2009-02-01	37	2.58	3.40	10.6	*C*	Grice et al. (2017)
87	2009-02-02	77	2.58	3.40	10.4	*C*	Grice et al. (2017)
88	2009-02-16	46	2.50	3.42	7.5	*C*	Grice et al. (2017)
89	2009-02-18	85	2.50	3.42	7.1	*C*	Grice et al. (2017)
90	2009-02-19	46	2.49	3.42	7.0	*C*	Grice et al. (2017)
91	2009-02-21	81	2.49	3.42	6.7	*C*	Grice et al. (2017)
92	2009-02-21	84	2.49	3.42	6.7	*C*	Grice et al. (2017)
93	2009-02-22	47	2.49	3.42	6.6	*C*	Grice et al. (2017)
94	2009-02-22	63	2.49	3.42	6.6	*C*	Grice et al. (2017)
95	2009-02-26	40	2.48	3.42	6.2	*C*	Grice et al. (2017)
96	2009-02-27	48	2.48	3.42	6.1	*C*	Grice et al. (2017)
97	2009-03-01	50	2.48	3.43	6.1	*C*	Grice et al. (2017)
98	2009-03-02	83	2.48	3.43	6.1	*C*	Grice et al. (2017)
99	2009-03-04	55	2.49	3.43	6.1	*C*	Grice et al. (2017)
100	2009-03-13	93	2.51	3.44	7.0	*C*	Grice et al. (2017)
101	2009-03-14	65	2.51	3.44	7.2	*C*	Grice et al. (2017)
102	2009-03-16	53	2.52	3.44	7.6	*C*	Grice et al. (2017)
103	2009-03-17	61	2.53	3.44	7.7	*C*	Grice et al. (2017)
104	2009-03-19	64	2.54	3.44	8.1	*C*	Grice et al. (2017)
105	2009-03-20	47	2.54	3.44	8.3	*C*	Grice et al. (2017)
106	2009-03-20	79	2.54	3.44	8.3	*C*	Grice et al. (2017)
107	2009-03-21	42	2.55	3.44	8.5	*C*	Grice et al. (2017)
108	2009-03-21	71	2.55	3.44	8.5	*C*	Grice et al. (2017)
109	2009-03-22	49	2.55	3.44	8.8	*C*	Grice et al. (2017)
110	2009-03-22	76	2.55	3.44	8.7	*C*	Grice et al. (2017)
111	2009-03-23	65	2.56	3.44	8.9	*C*	Grice et al. (2017)
112	2009-03-28	85	2.59	3.45	10.0	*C*	Grice et al. (2017)
113	2009-03-29	83	2.60	3.45	10.2	*C*	Grice et al. (2017)
114	2009-03-30	36	2.61	3.45	10.4	*C*	Grice et al. (2017)

Table A.3. continued.

N	Epoch	N_p	Δ (AU)	r (AU)	φ (°)	Filter	Reference
115	2009-03-30	74	2.61	3.45	10.4	*C*	Grice et al. (2017)
116	2009-03-30	77	2.61	3.45	10.4	*C*	Grice et al. (2017)
117	2009-03-31	52	2.62	3.45	10.6	*C*	Grice et al. (2017)
118	2009-04-01	75	2.63	3.45	10.8	*C*	Grice et al. (2017)
119	2009-04-01	77	2.63	3.45	10.8	*C*	Grice et al. (2017)
120	2009-04-02	75	2.64	3.45	11.0	*C*	Grice et al. (2017)
121	2009-04-12	71	2.73	3.46	12.9	*C*	Grice et al. (2017)
122	2009-05-12	35	3.11	3.48	16.5	*C*	Grice et al. (2017)
123	2009-05-12	35	3.11	3.48	16.5	*C*	Grice et al. (2017)
124	2011-06-02	51	2.23	2.98	15.2	*C*	Grice et al. (2017)
125	2011-06-12	50	2.12	2.97	12.8	*C*	Grice et al. (2017)
126	2011-06-12	62	2.12	2.97	12.8	*C*	Grice et al. (2017)
127	2011-06-13	57	2.11	2.97	12.5	*C*	Grice et al. (2017)
128	2011-06-13	74	2.11	2.97	12.5	*C*	Grice et al. (2017)
129	2011-06-20	41	2.04	2.96	10.4	*C*	Grice et al. (2017)
130	2011-06-21	40	2.03	2.95	10.1	*C*	Grice et al. (2017)
131	2011-07-08	39	1.93	2.93	4.5	*C*	Grice et al. (2017)
132	2011-07-09	47	1.93	2.93	4.1	*C*	Grice et al. (2017)
133	2011-07-09	69	1.93	2.93	4.2	*C*	Grice et al. (2017)
134	2011-07-10	41	1.92	2.93	3.8	*C*	Grice et al. (2017)
135	2011-07-10	79	1.92	2.93	3.8	*C*	Grice et al. (2017)
136	2011-07-18	41	1.90	2.91	2.5	*C*	Grice et al. (2017)
137	2011-07-31	39	1.91	2.89	6.0	*C*	Grice et al. (2017)
138	2011-08-01	39	1.91	2.89	6.4	*C*	Grice et al. (2017)
139	2011-08-06	45	1.93	2.89	8.1	*C*	Grice et al. (2017)
140	2012-09-17.0	151	2.05	2.62	20.6	*C*	K. Sobkowiak, Borowiec, Poland
141	2012-09-18.9	17	2.03	2.62	20.3	*C*	J. Nadolny, Borowiec, Poland
142	2012-09-24.0	10	1.98	2.62	19.4	*C*	J. Nadolny, Borowiec, Poland
143	2012-10-01.0	83	1.91	2.63	18.1	*C*	M. Bronikowska, Borowiec, Poland
144	2012-11-29.9	45	1.75	2.67	9.3	*C*	Francisco Soldan
145	2012-12-01.9	48	1.76	2.67	9.8	*C*	Francisco Soldan
146	2012-12-02.9	59	1.77	2.68	10.1	*C*	Francisco Soldan
147	2012-12-08.9	29	1.81	2.68	11.7	*C*	Francisco Soldan
148	2012-12-26.0	18	1.96	2.70	16.1	*C*	Francisco Soldan
149	2012-12-26.0	24	1.96	2.70	16.1	*C*	Francisco Soldan
150	2012-12-26.8	174	1.97	2.70	16.3	*C*	Francisco Soldan
151	2012-12-27.8	145	1.98	2.70	16.6	*C*	Francisco Soldan
152	2012-12-28.8	23	1.99	2.70	16.8	*C*	Francisco Soldan
153	2012-12-28.8	55	1.99	2.70	16.8	*C*	Francisco Soldan
154	2016-05-23.1	52	2.27	3.18	9.3	*C*	Raul Melia, Cordoba, Argentina
155	2016-06-15.1	52	2.14	3.15	2.3	*C*	Carlos Colazo, Cordoba, Argentina
156	2016-06-16.2	42	2.14	3.15	2.1	*C*	Carlos Colazo, Cordoba, Argentina
157	2016-07-25.9	51	2.26	3.09	12.9	*C*	A. Marciniak, Obs. del Teide, Spain
158	2017-07-16.4	149	2.22	2.62	22.3	*V*	Warner (2018)
159	2017-07-17.4	172	2.21	2.62	22.2	*V*	Warner (2018)
160	2017-07-18.4	156	2.20	2.62	22.2	*V*	Warner (2018)
161	2017-07-21.4	201	2.16	2.62	22.0	*V*	Warner (2018)
162	2017-07-22.4	196	2.15	2.62	21.9	*V*	Warner (2018)
163	2017-07-23.0	29	2.14	2.62	21.8	*r*'	R. Szakats, Piszkes Obs., Hungary
164	2017-08-01.0	47	2.04	2.61	20.9	*C*	Adrian Jones, *Gaia*-GOSA
165	2017-08-12.0	23	1.93	2.61	19.3	*R*	R. Szakats, Piszkes Obs., Hungary
166	2017-08-14.0	35	1.91	2.61	19.0	*R*	R. Szakats, Piszkes Obs., Hungary
167	2017-08-15.1	17	1.90	2.60	18.8	*R*	R. Szakats, Piszkes Obs., Hungary
168	2017-08-16.0	66	1.89	2.60	18.6	*R*	R. Szakats, Piszkes Obs., Hungary
169	2017-10-11.9	38	1.67	2.59	11.1	*r*'	R. Szakats, Piszkes Obs., Hungary
170	2017-10-16.8	139	1.69	2.59	11.8	*R*	R. Duffard, La Sagra, Spain
171	2017-11-08.9	154	1.83	2.59	16.8	*R*	R. Duffard, La Sagra, Spain
172	2017-11-15.9	276	1.89	2.59	18.2	*R*	R. Duffard, La Sagra, Spain
173	2017-11-16.9	188	1.90	2.59	18.4	*R*	R. Duffard, La Sagra, Spain

Table A.3. continued.

N	Epoch	N_p	Δ (AU)	r (AU)	φ (°)	Filter	Reference
174	2017-12-4.0	76	2.07	2.59	20.9	*C*	D. Molina, *Gaia*-GOSA
175	2017-7-14.1	58	2.25	2.62	22.4	*C*	D. Molina, *Gaia*-GOSA
176	2017-7-16.2	63	2.22	2.62	22.3	*C*	D. Molina, *Gaia*-GOSA
177	2017-7-23.2	48	2.14	2.62	21.8	*C*	D. Molina, *Gaia*-GOSA
178	2017-7-26.2	35	2.11	2.62	21.6	*C*	D. Molina, *Gaia*-GOSA
179	2017-7-27.2	58	2.10	2.62	21.5	*C*	D. Molina, *Gaia*-GOSA
180	2017-8-6.1	187	1.99	2.61	20.3	*C*	A. Jones, *Gaia*-GOSA
181	2018-12-09.1	83	2.22	3.01	13.2	*V*	C. Garcia, *Gaia*-GOSA
182	2018-12-10.1	100	2.21	3.01	13.0	*V*	C. Garcia, *Gaia*-GOSA
183	2018-12-14.0	54	2.18	3.01	11.8	*V*	C. Garcia, *Gaia*-GOSA
184	2018-12-3.3	1395	2.28	3.00	14.8	Rc	E. Jehin, M. Ferrais, TRAPPIST-N and -S
185	2019-1-16.2	540	2.09	3.06	2.1	Rc	E. Jehin, M. Ferrais, TRAPPIST-S
186	2019-1-19.2	492	2.09	3.07	2.7	Rc	E. Jehin, M. Ferrais, TRAPPIST-S
187	2019-1-26.3	811	2.12	3.08	4.9	Rc	E. Jehin, M. Ferrais, TRAPPIST-S
188	2019-2-1.2	269	2.16	3.09	7.0	Rc	E. Jehin, M. Ferrais, TRAPPIST-S
189	2019-1-16.1	269	2.09	3.06	2.1	*r*'	M. Person, T. Brothers
190	2012-12 – 2018-1	198				*V*	ASAS-SN
191	2015-1 – 2016-4	16				*V*	*Gaia* DR2

Table A.4. Mass estimates ($\mathcal{M}$) of (704) Interamnia collected in the literature.

#	Mass ($\mathcal{M}$) (kg)	Method	Sel.	Reference
1	$(7.36 \pm 3.38) \times 10^{19}$	DEFL	✓	Landgraf (1992)
2	$12.3^{+13.1}_{-12.3} \times 10^{19}$	DEFL	✗	Vasiliev & Yagudina (1999)
3	$(2.59 \pm 0.14) \times 10^{19}$	DEFL	✓	Krasinsky et al. (2001)
4	$(7.00 \pm 1.85) \times 10^{19}$	DEFL	✓	Michalak (2001)
5	$(1.61 \pm 0.84) \times 10^{19}$	DEFL	✗	Chernetenko & Kochetova (2002)
6	$(1.61 \pm 0.84) \times 10^{19}$	DEFL	✗	Kochetova (2004)
7	$(7.12 \pm 0.84) \times 10^{19}$	DEFL	✗	Baer & Chesley (2008)
8	$(11.30 \pm 3.18) \times 10^{19}$	DEFL	✗	Ivantsov (2008)
9	$(3.23 \pm 0.02) \times 10^{19}$	EPHEM	✓	Fienga et al. (2009)
10	$(3.69 \pm 0.37) \times 10^{19}$	EPHEM	✓	Folkner et al. (2009)
11	$(2.66 \pm 1.09) \times 10^{19}$	DEFL	✓	Somenzi et al. (2010)
12	$(3.88 \pm 0.18) \times 10^{19}$	DEFL	✓	Baer et al. (2011)
13	$(3.97 \pm 1.31) \times 10^{19}$	EPHEM	✓	Konopliv et al. (2011)
14	$(2.25 \pm 0.66) \times 10^{19}$	DEFL	✓	Zielenbach (2011)
15	$(3.34 \pm 0.52) \times 10^{19}$	DEFL	✓	Zielenbach (2011)
16	$(3.13 \pm 0.52) \times 10^{19}$	DEFL	✓	Zielenbach (2011)
17	$(3.88 \pm 0.75) \times 10^{19}$	DEFL	✓	Zielenbach (2011)
18	$(3.82 \pm 0.36) \times 10^{19}$	EPHEM	✓	Fienga et al. (2011)
19	$(3.82 \pm 0.47) \times 10^{19}$	EPHEM	✓	Fienga et al. (2013)
20	$(3.94 \pm 0.69) \times 10^{19}$	EPHEM	✓	Kuchynka & Folkner (2013)
21	$(2.43 \pm 0.19) \times 10^{19}$	EPHEM	✓	Pitjeva (2013)
22	$(3.82 \pm 0.41) \times 10^{19}$	EPHEM	✓	Fienga et al. (2014)
23	$(2.72 \pm 0.12) \times 10^{19}$	DEFL	✓	Goffin (2014)
24	$(3.42 \pm 0.18) \times 10^{19}$	DEFL	✓	Kochetova & Chernetenko (2014)
25	$(4.18 \pm 0.44) \times 10^{19}$	EPHEM	✓	Viswanathan et al. (2017)
26	$0.31^{0.80}_{-0.31} \times 10^{19}$	DEFL	✗	Siltala & Granvik (2017)
27	$(4.38 \pm 0.24) \times 10^{19}$	EPHEM	✓	Baer & Chesley (2017)
	$(3.79 \pm 1.28) \times 10^{19}$	Average		

Notes. For each, the 1σ uncertainty, method, selection flag, and bibliographic reference are reported. The methods are DEFL: Deflection, EPHEM: Ephemeris.